Adaptive Control of a Tilt Mirror for Laser Beam Steering*

Byung-Sub Kim
Intelligence and Precision Machine Department
Korea Institute of Machinery and Materials
Daejeon, 305-343, Korea
bkim@kimm.re.kr

Steve Gibson and Tsu-Chin Tsao
Mechanical and Aerospace Engineering
University of California
Los Angeles, CA 90095-1597
gibson@ucla.edu, ttsao@seas.ucla.edu

***Abstract*— This paper presents design and experimental implementation of an adaptive control system for a two-axis tilt mirror for laser beam steering. Disturbances in the laser beam are rejected by an optimal H_∞ feedback controller augmented by an adaptive control loop that identifies control gains that are optimal for the disturbance acting on the laser beam. Identification and control algorithms are applied to a laboratory beam-steering system at UCLA. In the adaptive control loop, an adaptive lattice filter implicitly identifies the disturbance statistics from real-time sensor data. The experimental results demonstrate that the adaptive controller used to augment H_∞ controller achieves substantially better disturbance rejection than does the H_∞ controller alone.**

I. INTRODUCTION

Laser beam steering or pointing, which refers to active control of the beam direction to stabilize the beam image at a desired remote point, is a critical function in many applications, including optical communications systems, astronomy, and directed energy systems. Beam steering control loops, usually called track loops, are critical components in adaptive optics systems, which compensate for wavefront distortion produced by the medium, such as a turbulent atmosphere, through which a laser beam propagates. A two-axis mirror in the beam path can be used to steer the beam to compensate for the atmospheric disturbances.

Substantial research has been conducted on modeling atmospheric disturbances [1]–[5]. Adaptive optics applications often require the adaptive optics loops, which use deformable mirrors and wavefront sensors to correct the higher-order turbulence effects on optical wavefronts, to have bandwidths of several hundred Hz. However, in both adaptive optics systems and wireless optical communications, the track loops with tilt mirrors like those in this paper normally are used to correct pointing errors below 30 Hz.

To compensate dynamic disturbances effectively, the beam steering control system must have either a much larger bandwidth than the disturbance bandwidth, typically ten times more, or a bandwidth comparable to that of the disturbance but with the ability to estimate adaptively the dynamic characteristics of disturbances. Integral feedback control commonly has been used in the track loop of adaptive optics systems, and it represents the former approach. The adaptive approach is more attractive because the expense of high-bandwidth actuator and servo control mechanisms can be saved by employing more sophisticated estimation and control schemes.

* This research was supported by AFOSR Grant F49620-02-01-0319.

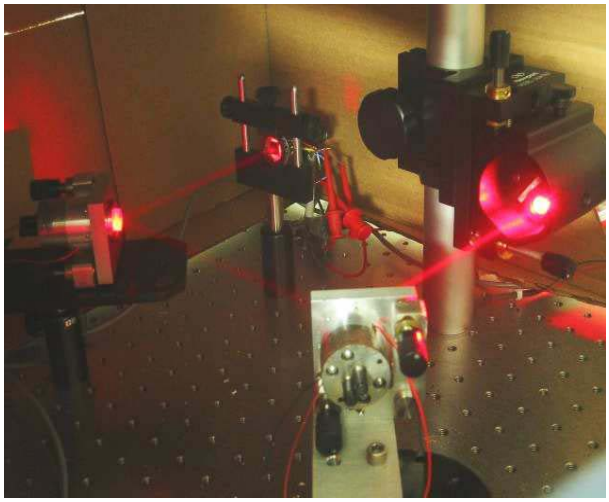

Fig. 1. UCLA adaptive beam steering experiment. The laser beam leaves the source on the right side in the picture, reflects off beam steering mirror 1 (the control actuator), then reflects off beam steering mirror 2 (the disturbance actuator, left side in the picture), and finally hits the quad cell in the top of the picture.

In this paper, we apply both an H_∞ feedback control loop and an adaptive control loop to reject disturbance added to the direction of a laser beam. In our adaptive loop, an adaptive lattice filter implicitly identifies the disturbance statistics from real-time quad cell data and computes optimal feedforward control gains.

II. EXPERIMENTAL SYSTEM DESCRIPTION

An experimental system was constructed at UCLA to test laser beam steering control algorithms. The optical system shown in Figure 1 consists of a laser source, a tilt mirror used as a beam steering control actuator, another tilt mirror used as a disturbance actuator, and a quad cell photo detector, which senses the position of the incident light. Each tilt mirror is mounted on a gimbaled mechanism driven by two piezoelectric actuators.

As shown in Figure 1, the laser beam leaves the source on the right side in the picture, reflects off beam steering

mirror 1 (the control actuator), then reflects off beam steering mirror 2 (the disturbance actuator, left side in the picture), and finally hits the quad cell in the top of the picture.

In our experimental set-up, the disturbance actuator is driven by a separate open-loop control system using a Texas Instrument C32 digital signal processor to inject sinusoidal and/or random disturbances to the track loop. The counteracting control system for the beam steering control actuator consists of a floating point digital signal processor (Texas Instrument C67), analog interfaces to the tilt mirrors and quad cell interface electronic circuit, and a personal computer. The real-time control algorithms are implemented by the DSP in single precision floating point computation, while the adaptive controller's parameter identification algorithm is performed in double precision on the PC. The communication between the DSP and PC is done through a 32-bit RAM area (single precision). A graphical user interface has been developed to facilitate real-time data acquisition and visualization through a bi-directional communication channel between the DSP and PC.

While the real-time control algorithm runs on the C67 DSP at a 2 KHz sampling rate, a set of 4000 data points from each sensor axis (i.e., two seconds of data) is collected and transferred to the PC by the user interface program. Then the lattice-filter based parameter identification program on the PC identifies an optimal feedforward FIR filter, which is the main component of the adaptive control loop. When the parameter identification program finishes computation, the user interface program writes the new adaptive filter to the C67 DSP control loop without interrupting the real-time operation of the control loop. The user interface program not only displays the laser beam trajectories on the computer screen in real time, but also commands the cyclic procedure of transferring data between the DSP and PC and updating FIR gains.

Since the parameter identification part is constructed as a SIMULINK® block on the PC, different adaptation algorithms can be tested without modifying the C67 DSP control loop in our set-up. Furthermore, the parameter identification program can be used without modification in SIMULINK simulations of the experiment. It is also possible to implement both the real-time control algorithm and the adaptive identification algorithm both on a DSP.

III. CONTROL LOOPS

In typical beam steering applications, including adaptive optics, the plant dynamics of the control actuators are known but the disturbance dynamics, which are dependent on the atmospheric conditions of the light path, are unknown. For the experiment described in this paper, the plant dynamics are identified from input/output data before the control loop is designed. Therefore, the adaptive control algorithm presented in this paper assumes known LTI plant dynamics but unknown disturbance dynamics.

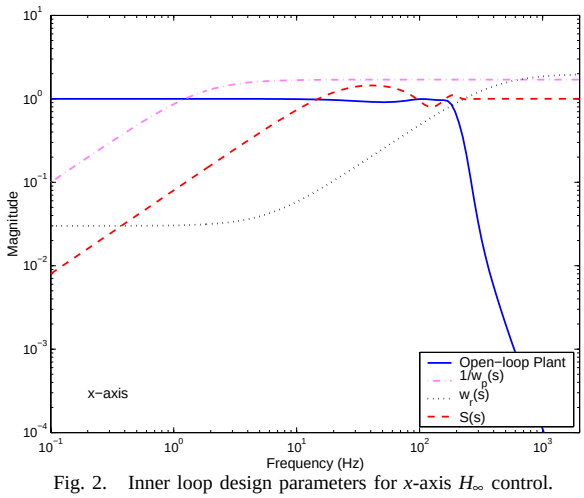

Fig. 2. Inner loop design parameters for x-axis H_∞ control.

A. H_∞ *Track Loop*

To compensate for nonlinearities in the quad-cell detector, gimbal mechanism, and hysteresis in the piezoelectric actuators, and to reduce sensitivity to temperature variations, an inner feedback control loop was introduced. This inner loop employed an H_∞ robust controller at 2 kHz sampling frequency. Anti-aliasing analog low-pass filters were introduced and modeled as part of the actuator dynamics.

A mixed sensitivity problem was solved to design an H_∞ controller in continuous-time and the resulting continuous-time controller was converted to a discrete-time model. The mixed sensitivity specification for H_∞ control design in continuous-time was

$$\|N\|_\infty = \max_\omega \bar{\sigma}(N(j\omega)) < 1, \quad N = \begin{bmatrix} w_p(s)S(s) \\ w_u(s)K(s)S(s) \end{bmatrix}, \quad (1)$$

where $S(s)$ is the sensitivity function, $K(s)$ is the desired H_∞ controller, $1/|w_p(s)|$ and $1/|w_u(s)|$ put upper bounds on the magnitude of $S(s)$ (for performance) and $K(s)S(s)$ (to penalize large inputs), respectively. The H_∞ optimal controller was obtained by solving the problem

$$\min_{K(s)} \|N(K)\|_\infty. \quad (2)$$

The saturation limit on the piezoelectric actuator control signal was ± 4 Volts, so we penalized the magnitude of the control signal using $w_u(s) = 4$. Figure 2 shows other design parameters used in the x-axis inner loop control design and the final sensitivity function from the computed H_∞ controller. The function $w_r(s)$ in Figure 2 is the input multiplicative uncertainty of the open-loop plant model, which was used in robustness tests. The robust performance and stability μ-values were 0.954 and 0.125, respectively, in x-axis. This means that the inner feedback control loop is quite robust against the uncertainty of the open-loop plant. Another H_∞ controller was designed similarly and converted

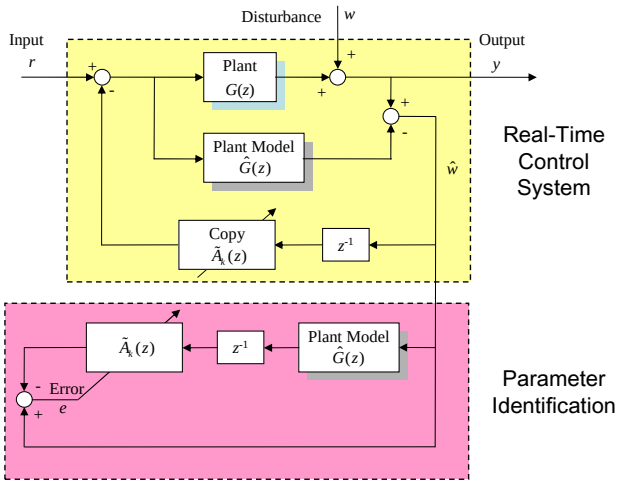

Fig. 3. Block diagrams for adaptive control and parameter-identification.

to a discrete-time controller for the y-axis. In our experiment, the H_∞ optimal control alone lends significant improvement over the conventional track loop (i.e., an integral feedback loop) implemented in most adaptive optics systems.

B. Adaptive Control Loop

Figure 3 shows the basic structure of the adaptive system for canceling plant disturbance. The closed-loop system consisting of the open-loop mirror/quad cell system and the H_∞ feedback loop is considered to be the plant $G(z)$ for purposes of adaptive control. The adaptive control algorithm uses the estimate $\hat{G}(z)$, determined as described in Section IV, instead of the true $G(z)$. The FIR filter $\tilde{A}_k(z)$ is the key component of the adaptive loop. The optimal FIR gains are identified from the real-time input/output data by the lattice filter running on the PC.

With the adaptive loop closed, the transfer function from the reference command r to the quad cell output y is

$$H_{ry}(z) = \frac{G(z)}{1+z^{-1}\tilde{A}_k(z)(G(z)-\hat{G}(z))}, \qquad (3)$$

and the transfer function from the disturbance w to y is

$$H_{wy}(z) = H_{we}(z) = \frac{1-z^{-1}\tilde{A}_k(z)G(z)}{1+z^{-1}\tilde{A}_k(z)(G(z)-\hat{G}(z))}. \qquad (4)$$

If the plant model $\hat{G}(z)$ is identical to the true plant $G(z)$, then $\tilde{A}_k(z)$ does not affect the stability of $H_{ry}(z)$ and $H_{wy}(z)$. Sufficiently large modeling error $G(z)-\hat{G}(z)$ can cause the system to be unstable with the adaptive loop closed. However, the model verification results in Section IV indicate that the modeling error is quite small in the bandwidth of interest in the experiment presented in this paper.

The transfer function from w to y is the same as the transfer function from w to e. It follows that if $\tilde{A}_k(z)$ is designed to minimize the effect of w on e, the effect of w will be minimized at the plant output y. Also, if the model $\hat{G}(z)$ is sufficiently close to the plant $G(z)$, then the optimal $z^{-1}\tilde{A}_k(z)$ is an approximate inverse of the plant $G(z)$ in the bandwidth of w.

As shown in Figure 3, the main component in the adaptive outer control loop is a two-input/two-output adaptive FIR filter $\tilde{A}_k(z)$, which are identified by a recursive least squares (RLS) lattice filter. For the experimental results presented in this paper, the FIR filter used four taps. Using more taps did not improve the performance for the disturbance bandwidths used.

The output of the FIR filter is the adaptive control command. The input to the FIR filter is the signal $\hat{w}$, which is an estimate of the disturbance. Since the control-loop designs are based on linear plant models, the disturbance is modeled as output disturbance, without loss of generality. The disturbance estimate $\hat{w}$ is computed by filtering the output of the FIR filter through the identified plant model $\hat{G}(z)$ and subtracting the resulting signal from the sensor signal, as shown in Figure 3. The dark shaded block in Figure 3 illustrates that the FIR filter gains, which implicitly represent the disturbance statistics, are identified by an adaptive filter. This adaptive filter is driven by the disturbance estimate $\hat{w}$ filtered through the plant model $\hat{G}(z)$. Similar adaptive disturbance rejection control and filtering loops have been used in applications to acoustic noise cancelation and vibration suppression [6].

The most significant difference between the algorithms used in this research and those used in classical noise cancelation is the use of and RLS lattice filter developed at UCLA [7] for identification of the optimal FIR gains. This unwindowed RLS lattice filter provides much faster convergence than do the LMS algorithms typically used in adaptive noise cancelation. An adaptive control algorithm based on a related stohchastic-gradient lattice filter has been applied to control of acoustic noise [8], but the experiment described here appears to be the first application of adaptive disturbance rejection in laser beam steering.

IV. SYSTEM IDENTIFICATION

The open-loop plant model for the transfer function from the actuator commands to the quad cell x and y outputs was obtained from experimental frequency response data. The frequency responses were measured with a dynamic signal analyzer using a swept sine method that generates fixed-amplitude sine waves of varying frequencies. From the frequency responses for different input amplitudes, an averaged frequency response was computed and a nominal continuous-time open-loop plant model was fitted.

The open-loop plant model was used to design a continuous-time H_∞ controller $K(s)$ for each mirror axis. Then $K(s)$ was converted to a discrete-time controller $K(z)$ for the 2 KHz sample and hold rate.

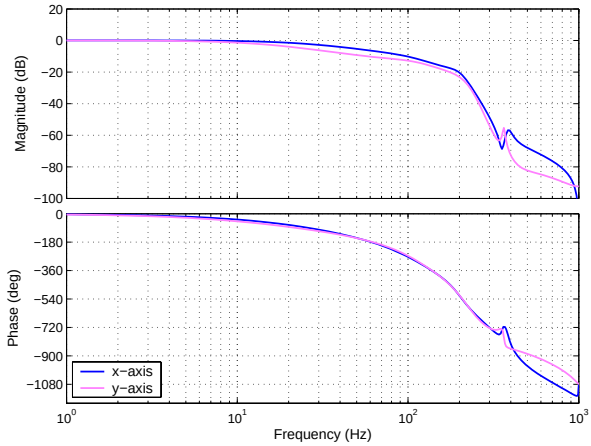

Fig. 4. Bode plots for identified beam steering system with H_∞ closed.

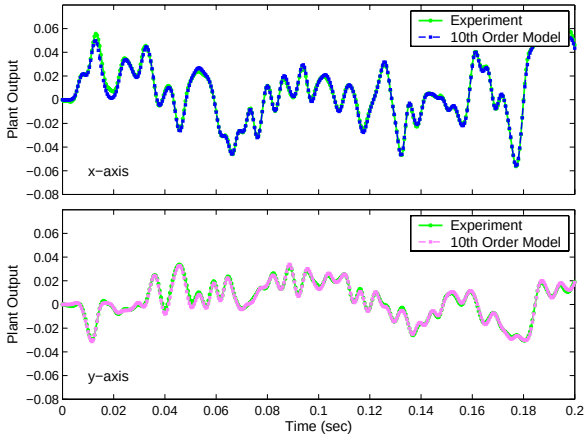

Fig. 5. Verification of identified plant model $\hat{G}(z)$.

With the two-channel H_∞ feedback loop closed, the mirror was driven with broadband reference command sequences to generate time-domain input/output data. This data was used in a subspace identification method [9] to determine a model $\hat{G}(z)$ of the two-input/two-output transfer function from augmenting mirror commands to the quad-cell outputs. The identified transfer function $\hat{G}(z)$ is an estimate of the transfer function $G(z)$ that represents the beam-steering system with the H_∞ feedback loop closed. (See Figure 3.) Figure 4 shows the Bode plots of $\hat{G}(z)$. The two mirror commands produce tilts about the x and y mirror axes. The Bode plots show that the plant with the H_∞ loop closed has a bandwidth of about 20 Hz. The identified $\hat{G}(z)$ has ten states in each channel.

Figure 5 shows excellent agreement between the measured output sequences and output sequences produced by filtering the experimental inputs through $\hat{G}(z)$. Hence this identified plant model should be sufficiently accurate for use in the adaptive control loop and parameter identification.

We also used the swept sine method to identify a closed-loop plant model $\hat{G}(z)$, but in the model verification, the model $\hat{G}(z)$ obtained by the swept sine method produced output sequences delayed by two steps relative to the output of the real plant output. The $\hat{G}(z)$ from the subspace algorithm displayed no such delay. Hence, we used the $\hat{G}(z)$ from subspace identification in the adaptive control algorithm.

V. EXPERIMENTAL CONTROL RESULTS

In the experiments, the disturbance actuator (beam steering mirror 2) added disturbance sequences in the form of tilts about both the x and y axes to the laser beam after it left the control actuator (beam steering mirror 1). With no control loops closed, the disturbance caused the centroid of the image of the beam on the quad cell to wander randomly with a nonzero mean positoin. Closed the H_∞ feedback loop eliminated the nonzero mean of the spot on the quad cell and reduced the variance of the motions slightly. After the adaptive loop was closed for approximately one second (after using two seconds of data to identify the optimal FIR gains), the variance of the motion of the laser spot on the quad cell was reduced substantially.

Figure 6 shows RMS values of the plant output and corresponding screen shots in the top when the disturbances are 10 Hz sinusoidal sequences. Each point on the RMS plot is the RMS value over the preceding 50 samples of the displacement of the centroid of the beam image from the center of the quad cell (i.e., the output error). We can see that the H_∞ loop alone eliminates drifting of the laser spot on the qual cell and reduces the disturbance quite well. Remarkably, when the adaptive-loop works with the H_∞ inner loop controller, the disturbances are hardly seen at the plant output. If the disturbance consists of a single sine wave with known frequency, a simple notch filter can cancel the disturbance as does the adaptive control in our experiment. However, in our experiment the optimal FIR filter was constructed adaptively without *a priori* information about the disturbance.

In the second experiment, the disturbances for the two axes were independent random sequences, each with a bandwidth of 20 Hz. Screen shots in the top of Figure 7 show representative sample trajectories of the centroid of the laser image on the quad cell in the experiment. As seen in the simple sinusoidal disturbance case, the H_∞ feedback control augmented by the adaptive loop substantially reduces the variance of the motion of the laser spot on the quad cell. The top right picture shows the trajectory for a period shortly after the adaptive loop is closed. These results demonstrate the enhanced beam control possible with the adaptive control scheme.

VI. CONCLUSIONS

We have applied an adaptive control algorithm to reject broadband and narrow-band disturbances in a laser beam steering experiment. In our adaptive loop, an RLS lattice filter implicitly identifies the disturbance statistics from real time quad cell data and computes optimal feedforward gains for an FIR filter. This adaptive loop augments a linear time-invariant H_∞ feedback control loop. The feedback loop eliminates drift and some beam jitter present in open-loop beam motion, but the adaptive loop achieves substantial performance enhancement over the feedback loop alone because the lattice filter optimizes the adaptive loop for the particular disturbance spectrum.

This research is continuing at UCLA, but already it has demonstrated the enhanced disturbance rejection achievable in laser beam steering by modern optimal feedback controllers augmented by adaptive control loops that determine control gains that are optimal for the current disturbance acting on the laser beam.

VII. REFERENCES

[1] M. C. Roggemann and B. Welsh, *Imaging Through Turbulence* , CRC, New York, 1996.

[2] R. K. Tyson, *Principles of Adaptive Optics*, Academic Press, New York, 1998.

[3] D. L. Fried, "Least-squares Fitting a Wave-front Distortion Estimate to an Array of Phase Difference Measurements", *J. Opt. Soc. Am.*, vol. 67, 1977, pp 370-375.

[4] B. L. Ellerbroek, "First-order Performance Evalution of Adaptive Optics Systems for Atmospheric Turbulence Compensation in Extended Field-of-view Astronomical Telescopes", *J. Opt. Soc. Am. A*, vol. 11, 1994, pp 783-805.

[5] R. Q. Fugate and B. L. Ellerbroek et al., "Two Generations of Laser Guide Star Adaptive Optics Experiments at the Starfire Optical Range", *J. Opt. Soc. Am. A*, vol. 11, 1994, pp 310–324.

[6] B. Widrow and E. Walach, *Adaptive Inverse Control*, Prentice Hall, Englewood Cliffs, NJ, 1996.

[7] S.-B. Jiang and J. S. Gibson, "An Unwindowed Multichannel Lattice Filter with Orthogonal Channels", *IEEE Transactions on Signal Processing*, vol. 43, no. 12, 1995, pp 2831-2842.

[8] S.-J. Chen and J. S. Gibson, "Feedforward Adaptive Noise Control with Multivariable Gradient Lattice Filters", *IEEE Transactions on Signal Processing*, vol. 49, no. 3, 2001, pp 511–520.

[9] P. Van Overschee and B. DeMoor, *Subspace Identification for Linear Systems: Theory-Implementation-Applications*, Kluwer Academic Publishers, 1996.

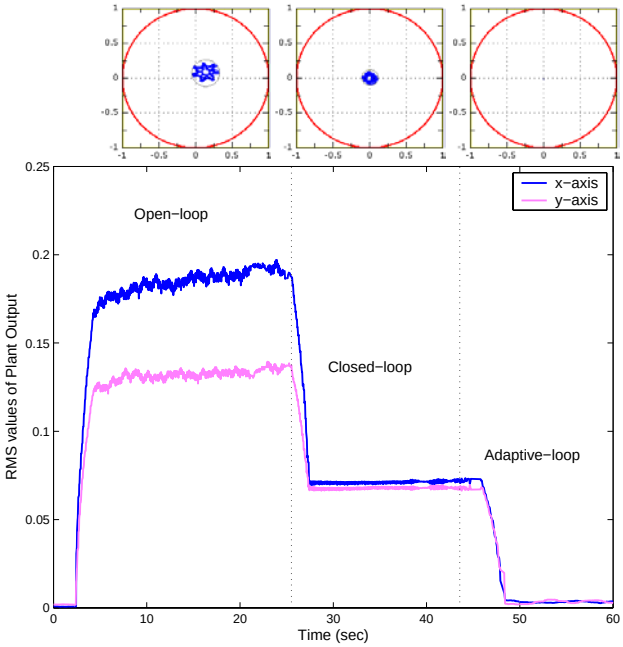

Fig. 6. Top: Screen shots of the laser-beam trajectories on the quad cell. Bottom: RMS values of the plant output when sinusoidal (10 Hz only) disturbances are injected. Top left: open loop. Top middle: H_∞ feedback control loop closed. Top right: adaptive control loop closed.

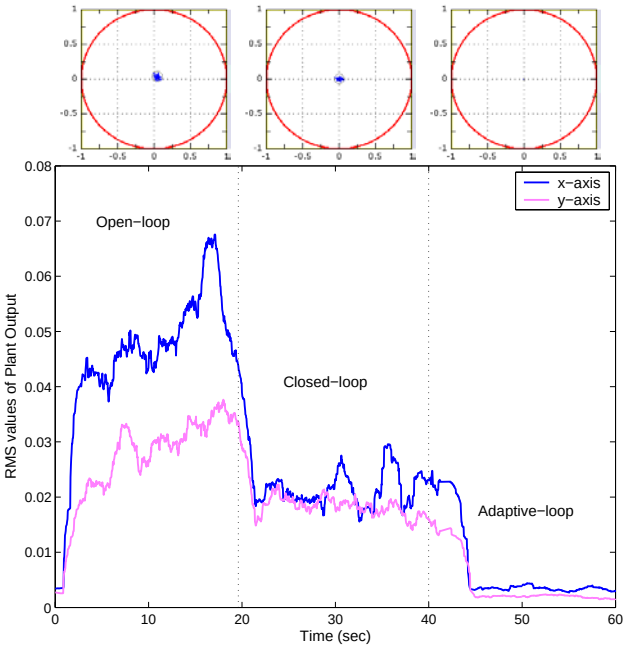

Fig. 7. Top: Screen shots of the laser-beam trajectories on the quad cell. Bottom: RMS values of the plant output when band-limited (20 Hz) random disturbances are injected. Top left: open loop. Top middle: H_∞ feedback control loop closed. Top right: adaptive control loop closed.